AIAA JOURNAL
Vol. 35, No. 1, January 1997

Hover Testing of Smart Rotor with Induced-Strain Actuation of Blade Twist

Peter C. Chen* and Inderjit Chopra†
University of Maryland, College Park, Maryland 20742

The experimental results are presented of a hover test with a one-eighth dynamically scaled (Froude scale) helicopter rotor model with embedded piezoceramic elements as actuators to suppress vibrations. A 6-ft-diam two-bladed bearingless rotor model was built with banks of piezoelectric torsional actuators capable of manipulating blade twist at harmonics of the rotational speed. The twist performances of several rotor blade configurations were investigated using accelerometers embedded in the blade tip. The change in oscillatory rotor lift due to piezoactuation was measured by a hub balance. Experimental results show that linear twist distributions of up to 0.6 deg, resulting in increases of up to 10% of the nominal rotor lift, are possible with existing piezoceramic technology. Although the twist amplitudes attained in this experiment were less than the target value (1–2 deg), it is expected that partial reduction of hub vibration can be achieved with the current smart rotors.

Nomenclature

b = width
d_{31} = piezoelectric constant
E = electric field
EI = bending stiffness
GJ = torsional stiffness
l = length
m = distributed mass
t = thickness
β = actuator orientation
ΔS = actuator spacing
θ_0 = rotor collective pitch angle
Λ = induced strain
λ = shear lag parameter
ϕ = rotation angle
φ = area stiffness ratio

Subscripts

b = beam reference
c = actuator reference
s = adhesive reference
sk = skin reference

Superscript

$\tilde{}$ = actuator axes reference

Introduction

HELICOPTERS suffer from high vibration, which not only affects the quality of the ride but also reduces the life expectancy of the rotor components due to high dynamic stresses. The primary source of helicopter vibration is the main rotor, which operates in an unsteady and complex aerodynamic environment. This causes aerodynamic forcing of the blades at higher harmonics of the rotational speed, which are transmitted to the fuselage as large oscillatory forces and moments. Typically, for an N-bladed rotor, the oscillatory ($N - 1$), N, and ($N + 1$) per revolution blade loads cause N per revolution forcing of the fuselage.[1] To reduce these vibrations to an acceptable level, helicopters routinely use passive and active vibration reduction devices. The passive vibration reduction systems either isolate (isolators) or diffuse (absorbers) the vibration source, but with a large weight penalty of up to 3% gross weight. Another drawback of passive devices is their rapid degradation in performance when the rotor is operated at conditions other than the tuned flight condition. In recent years, an active vibration control device, called the higher harmonic control (HHC), has been pursued vigorously to suppress the vibrations at the source. An HHC system excites the blade root pitch using the swashplate at higher harmonics of the rotational speed, generating new airloads that, in combination with the oscillatory inertial loads, cancel the blade loads that cause fuselage vibrations. The concept of HHC has been widely investigated by researchers using numerical simulations,[2,3] model testing in wind tunnels,[4] and full-scale testing.[5] Although this method has been proven to be quite effective to reduce vibration and causes a lower weight penalty (up to 1–2% of gross weight) than passive systems, a number of significant drawbacks exist. The power requirements of the servoactuators needed to drive the swashplate become substantial at extreme flight conditions, where vibrations are highest. Also, excitation frequencies of conventional HHC are limited to N/rev, where N is the number of blades. Other harmonics are needed to minimize blade stresses and to improve rotor performance.

To overcome many of these problems associated with the existing schemes of helicopter vibration reduction, considerable research has been directed toward the application of smart structures technology to rotorcraft systems. A smart structure, consisting of a substructure integrated with sensors, controllers, and actuators, is capable of achieving shape control as it is deformed. It has been proposed that modern smart materials such as piezoceramics, magnetostrictives, and electrostrictives may be used as actuators in helicopter vibration reduction systems for individual blade control (IBC).[6–12] Since pitch changes could be implemented to each individual blade of the rotor, control can be imposed over a much larger bandwidth than with current swashplate-based controls. This vibration reduction scheme could be comparatively more effective and efficient than conventional HHC systems. For the suppression of vibratory hub loads, it is necessary to excite blade tip twist on the order of 1–2 deg at frequencies of N/rev (where N is the number of blades). Other potential applications of this IBC scheme would include helicopter aeromechanical stability augmentation, handling qualities improvement, and reduction of acoustic signatures.

The concept of smart actuators/sensors distributed over the span of individual rotor blades is particularly attractive to manipulate

Received Jan. 18, 1995; presented as Paper 95-1097 at the AIAA 36th Structures, Structural Dynamics, and Materials Conference, New Orleans, LA, April 13–14, 1995; revision received Sept. 20, 1996; accepted for publication Sept. 30, 1996; also published in *AIAA Journal on Disc*, Volume 2, Number 2.

*Smart Structures Fellow, Department of Aerospace Engineering; currently Research Engineer, Systems Planning and Analysis, Inc., Alexandria, VA 22311-1712. Member AIAA.

†Professor and Director, Center for Rotorcraft Education and Research, Department of Aerospace Engineering. Fellow AIAA.

and sense the mechanical properties and the stress/strain field along the span of the blades. This allows for the use of control algorithms to modify and tune the closed-loop behavior of the blade. Because there are a large number of actuators in such a distributed control system, weight, complexity, and size of the actuators may alter the structural and dynamic properties of the blade. Small, lightweight piezoceramic (PZT) actuators are embedded in the outer skin of blade structures to allow for the application of localized strains through which the overall structural response of the blade could be changed. The use of these materials also offers the additional prospect of monitoring the structural damage of the rotor, enabling the pilot to take load alleviating action to minimize further damage.

To fully exploit the application of smart structures technology, it is necessary to develop the relevant analytical tools to predict the response of beams under induced-strain actuation. Pioneering work by Crawley and de Luis[13] presented a study on the bending/extension response of solid rectangular cross-sectional beams with surface-mounted or embedded distributed piezoceramic actuators. The analytical model captured the shear lag effect due to the finite bond layer in the surface-mounted actuators, whereas the embedded actuators were assumed to be perfectly bonded to the substrate. The normal strain throughout the actuator was assumed to be uniform across the thickness. The dynamic response of cantilevered beams due to sinusoidal excitation was validated by experiments. Crawley and Anderson[14] presented models of the detailed mechanics of the induced-strain actuation effect by piezoceramics. A comparison was made between the accuracy of the uniform strain model, Bernoulli–Euler model, and finite element analysis. Measured surface strains on the substructure and the actuator were used to validate these results. The Bernoulli–Euler model was found to be more accurate than the uniform strain model. Crawley and Lazarus[15] developed an analytical model based on classical laminated plate theory. The Rayleigh–Ritz technique was used to provide the solution for comparison. Park et al.[16] and Park and Chopra[17] formulated and experimentally verified a one-dimensional beam model to predict the coupled torsion/bending/extension of solid cross-sectional isotropic beams subject to surface-mounted piezoceramic actuators not aligned with respect to the beam axis. It was concluded that cross-sectional warping was negligible for thin isotropic beams, but the adhesive shear lag was a significant parameter that affected the torsional response. Although the detailed strain state was highly two-dimensional, experimental test results with actuators of an aspect ratio of 8 showed that the analytical model was acceptable to predict induced twist up to a 45-deg actuator orientation angle.

Chen and Chopra[18] examined the feasibility of a smart Froude-scale rotor and developed an analytical model to predict the twist and bending responses of closed-cell rotor blade models with embedded piezoceramic actuators. A one-dimensional uniform strain theory was formulated to predict the static response of rectangular section composite beams with embedded paired actuators that were not aligned with respect to the beam axis. Test specimens with variations in geometric parameters such as actuator orientation, actuator density, and actuator bond thickness were used to experimentally validate the model. At the operating speed of 900 rpm, a maximum tip twist of approximately 0.2 deg was achieved. Although this blade twist amplitude was 5–10 times less than what is required to suppress vibration, it demonstrated the potential feasibility of the concept and warranted continued research to improve the actuator design.

This paper continues to explore the feasibility of a controllable twist rotor using embedded single-layer and dual-layer piezoceramic actuators. Rotor blades with various actuator geometries were constructed and tested on a hover tower to determine the effect of rotation on piezoactuators. First, the details of model fabrication are presented. Then, the static nonrotating responses of the blades are measured and compared with theoretical predictions. Third, the rotating dynamic response of the blades are measured using accelerometers embedded in the blades. Finally, the aerodynamic effectiveness of the smart rotor is assessed by measuring the change in oscillatory lift due to piezoactuated blade twist at higher harmonics of the rotational speed.

Table 1 Froude-scale rotor blade properties

Property	Froude-scale target
Flap stiffness EI	1627 lb-in.^{2}
Torsional stiffness GJ	1708 lb-in.^{2}
Distributed mass m	0.0174 lbm/in.

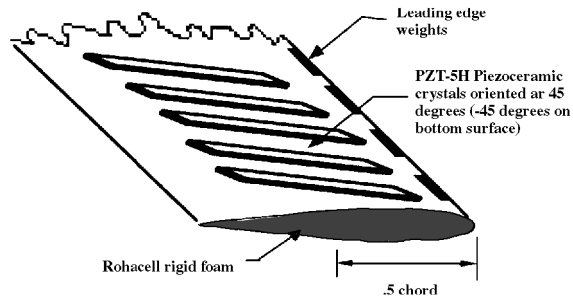

Fig. 1 Piezoceramic blade cross-sectional detail.

Model Fabrication

The smart rotor blade model under development is constructed by laminating 10-mil pre-preg fiberglass cloth plies around a rigid foam core that is cured in a NACA 0012 airfoil mold (Fig. 1). The overall blade length is 26.58 in. from tip to root and the chord is 3.0 in. Inertial coupling between the flap and pitch modes is reduced by placing the airfoil section c.g. at quarter-chord using tantalum leading-edge weights. To activate blade motion independently in bending and torsion and to sense blade deformations, two separate actuator configurations were examined (11.5-mil single-layer actuators and 23-mil dual-layer actuators). These specially shaped configurations are embedded under the fiberglass skin in banks of discrete actuators at angles of ± 45 deg on the top and bottom surfaces of the blade, respectively. The piezoceramic actuators are cut to dimensions of 2.0 in. in length and 0.25 in. in width to minimize transverse actuation. The dual-layer actuators are manufactured in-house by bonding two single-layer PZTs using a high-temperature cyanoacrylate (CA) adhesive. Electrical access to both layers is obtained by soldering wires to the outer surfaces and to the common electrode at the interface. A twist distribution along the blade span is achieved through in-phase excitation of the top and bottom actuators at equal potentials, while a bending distribution is achieved through out-of-phase excitation. The piezoceramic elements used for this research are lead zirconate titanate (PZT-5H) piezoceramics manufactured by Morgan Matroc, Inc.[19]

Four rotor configurations were built with varying actuator geometries to study the effect of actuator spacing and actuator thickness on the blade torsional response. The actuator spacing dimension is the distance between the adjacent edges of the actuators. Configurations 1A and 1B consist of single-layer PZTs with actuator spacings ΔS of 1.5 and 0.75 in., respectively, whereas 2A and 2B consist of dual-layer PZTs with actuator spacing ΔS of 1.5 and 0.75 in., respectively. The actuator bond thickness of all of the rotor blades was maintained at the minimal possible value (0.0025 in.) with the current manufacturing process to maximize shear transfer and, hence, actuation efficiency. Two matching blades were constructed for each configuration for hover testing. A number of actuator pairs were damaged during the molding process, rendering them ineffective in producing blade twist. The actuator geometries and the number of functional actuator pairs for each blade are listed in Table 1, along with the target and measured structural stiffness values of the rotor blades.

Static Response Testing

Analysis

The current authors[18] developed and experimentally verified a uniform strain analysis of the static response of composite rotor blades under induced-strain piezoactuation. In this analysis, torsional and bending deformations of a rectangular composite beam with one pair of PZTs oriented at $\pm\beta$ angles with respect to the

beam axis was investigated. It was determined that the behavior of a high aspect ratio structure, such as a rotor blade, could be adequately characterized using this one-dimensional beam theory. Although the torsional actuation mechanism is inherently a two-dimensional phenomenon, it was shown that high aspect ratio actuators allow for the mathematical simplification of assuming negligible transverse actuation. The limitations of this theory, which reduces two-dimensional piezoceramic effects to a one-dimensional model, were addressed by experimental test specimens with various actuator spacing. It was determined that actuators with close spacing introduced interaction effects that acted to reduce actuator authority and, hence, to reduce twist response. In this study, the piezoceramic actuators used in model fabrication had an aspect ratio of 8 to minimize two-dimensional effects. These actuators are assumed to act as one-dimensional line elements that produce a localized bending moment or torque about the midplane of the blade. The strain distribution is assumed to be uniform through the actuator thickness and linear through the beam and adhesive thickness. To manipulate twist response of the blade, equal in-phase excitation voltage potentials were applied to top and bottom actuators.

The twist response of the cantilevered blade due to excitation by one pair of embedded actuators oriented at $\pm\beta$ angles with respect to the beam axis was given in Ref. 18 as

$$\phi_b(\tilde{x}) = \frac{2\Lambda G_s b_c t_s \psi_{sk} \sin\beta[t_s + t_c + (t_b/2)]}{(GJ_b)\psi_s(\psi_{sk} + \cos^3\beta)} \times\left[\frac{\sinh(\lambda\tilde{x})}{\lambda\cosh\Gamma} + \frac{\tanh\Gamma}{\lambda} - \tilde{x} - \frac{l_c}{2}\right] \tag{1}$$

which is expressed as a function of the actuator free strain

$$\Lambda = d_{31}E \tag{2}$$

The skin and adhesive stiffness parameters are

$$\psi_{sk} = \frac{E_{sk}t_{sk}b_{sk}}{E_c t_c b_c} \tag{3}$$

$$\psi_s = \frac{E_s t_s b_s}{E_c t_c b_c} \tag{4}$$

and the additional shear lag parameters

$$\lambda^2 = \frac{\psi_s}{t_s^2}\left(\frac{\psi_{sk} + \cos^3\beta}{\psi_{sk}}\right) \tag{5}$$

$$\Gamma = \lambda(l_c/2) \tag{6}$$

Rotor Blade Structural Properties

The structural properties of the rotor blades were determined experimentally by measuring the spanwise bending and twist distributions along the blade under mechanical loading. A laser beam was reflected off mirrors mounted at the elastic axis (located at 0.28 chord) along the span of the blade to determine average values for the structural stiffness. The target values of bending stiffness EI, torsional stiffness GJ, and distributed mass m for a one-eighth Froude-scale rotor blade are listed in Table 1. The configuration parameters and the measured values of the smart rotor blades are listed in Table 2.

The measured structural stiffnesses vary somewhat from the desired Froude-scale target values. Although the actuator configurations varied from single- to dual-layer actuators, the target values for both configurations remain the same. The trends in measured blade stiffness values indicate that a decrease in the spacing of the actuators to one-half causes a larger increase in structural stiffness than an increase in the actuator thickness from one layer to two layers.

In general, an increase in the total number of actuators is observed to result in an increase in the structural stiffness of the blade. This behavior is exhibited by blade sets with single-layer actuators (1A and 1B), as well as sets with dual-layer actuators (2A and 2B). For set 1A and 1B, average increases in flap and torsional stiffnesses of approximately 21 and 18%, respectively, occur when the number of single-layer actuators is increased from 12 to 30 pairs. Similarly, for set 2A and 2B, average increases of approximately 23 and 22% in flap and torsional stiffnesses, respectively, occur when the number of dual-layer actuators is increased from 12 to 30 pairs.

Table 2 Rotor blade actuator configurations and measured structural stiffnesses

Blade no.	PZT type	ΔS, in.	Total pairs	Active pairs	EI, lb-in.^{2}	GJ, lb-in.^{2}	m, lbm/in.
1A1	Single	1.50	12	12	1380	1650	0.0103
1A2	Single	1.50	12	12	1359	1632	0.0101
1B1	Single	0.75	30	30	1768	2058	0.0129
1B2	Single	0.75	30	30	1697	1906	0.0103
2A1	Dual	1.50	12	11	1435	1758	0.0125
2A2	Dual	1.50	12	11	1484	1854	0.0126
2B1	Dual	0.75	30	25	1925	2348	0.0172
2B2	Dual	0.75	30	24	1886	2298	0.0171

An increase in stiffness results as the actuator thickness is doubled. An increase in actuator thickness (from 11.5 to 23 mil) for blade sets 1A and 2A result in an average increase of 6 and 10% in flap and torsional stiffnesses, respectively. Doubling actuator thickness from blade sets 1B to 2B result in an average increase of 10 and 14% in flap and torsional stiffnesses, respectively.

Overall, the range of stiffness variation is bounded by blades 1A2 and 2B1, which were found to have the smallest and largest structural stiffnesses, respectively. The range of deviation in bending stiffness EI of all eight blades was measured to be from approximately -16 to $+18\%$ from the target values for blades 1A2 and 2B1, respectively. The range of deviation in torsional stiffness GJ of all eight blades was measured to be from approximately -4 to $+37\%$ from the target values for blades 1A2 and 2B1, respectively. Keeping in view the complexity of the fabrication process, this range of variation is acceptable for the present investigation. The distributed mass of the blades approaches the target value as the total number of actuators is increased. Blades 1A2 and 2B1 were measured to be the lightest and heaviest, respectively, of the all of the blades. The distributed mass m increases from 1.7 times less to almost exactly the target value as the number and thickness of the actuators is increased.

Rotor Blade Static Response

For static free (no externally applied loads) response testing, the blades were cantilevered at the root and dc actuation potentials of 50, 75, 100, 125, and 150 V were applied to the actuators to induce a linear twist distribution along the span of the blade. A mirror/laser optics system was used to measure the deflections about the elastic axis at the tip of the blade. A correction factor based on block force analysis of overlapping actuators[20] was used to satisfactorily predict the twist response for the rotor blade configurations in this study with ΔS less than 1.5 in. The measured blade static twist response data are shown in Figs. 2 and 3, along with the analytical predictions.

The measured twist responses shows good correlation with theoretical predictions for all blades. The increase in torsional response with increasing voltage is accurately captured by the analytical model. The magnitudes of the experimental results are overpredicted by a maximum of 20% for all blades.

The nonrotating free torsional response is observed to be inversely proportional to the blade stiffness GJ. It is therefore desirable to maintain blade stiffness at the lowest possible values to maximize actuator authority. However, due to other dynamic considerations (e.g., Froude scaling parameters), the blade stiffnesses cannot be reduced beyond certain values.

Hover Testing

Rotor Structural Properties

To assess the effectiveness of the smart blade in the rotating condition, the blades were tested in a two-bladed bearingless rotor configuration (Fig. 4) on a hover tower. The natural frequencies of the four rotor configurations were experimentally determined by impulse response tests using a fast Fourier transform (FFT) spectrum analyzer. To measure the time response, an accelerometer was

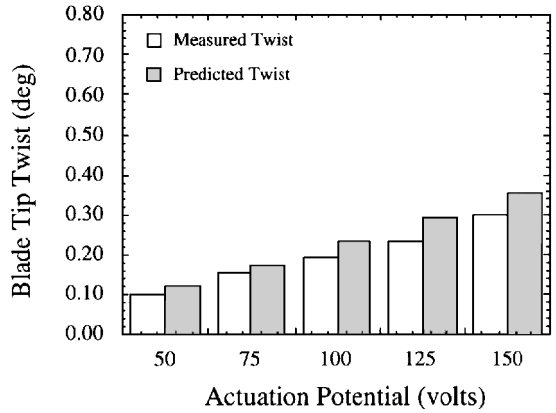

a) Blade 1A1 (ΔS = 1.5 in.)

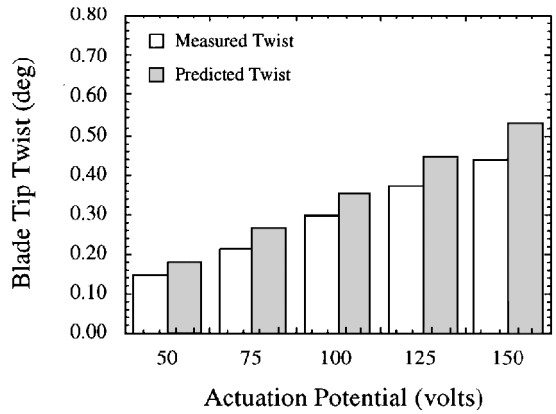

b) Blade 1A2 (ΔS = 1.5 in.)

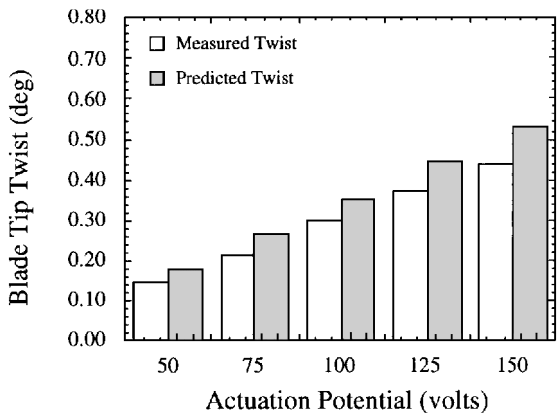

c) Blade 1B1 (ΔS = 0.75 in.)

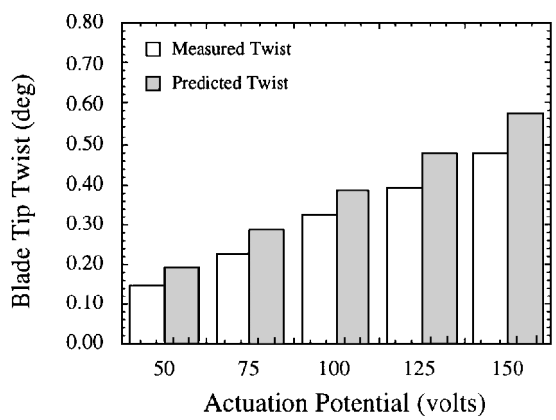

d) Blade 1B2 (ΔS = 0.75 in.)

Fig. 2 Static-induced torsional response of blades with single-layered actuators.

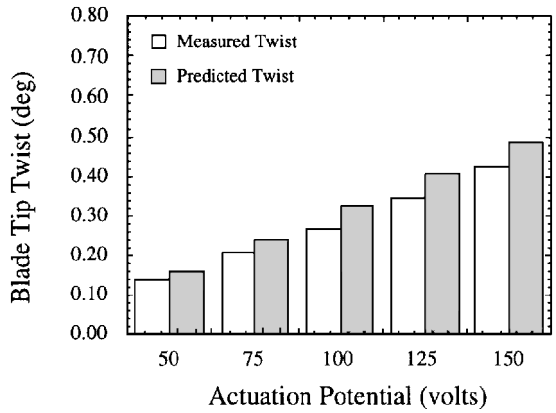

a) Blade 2A1 (ΔS = 1.5 in.)

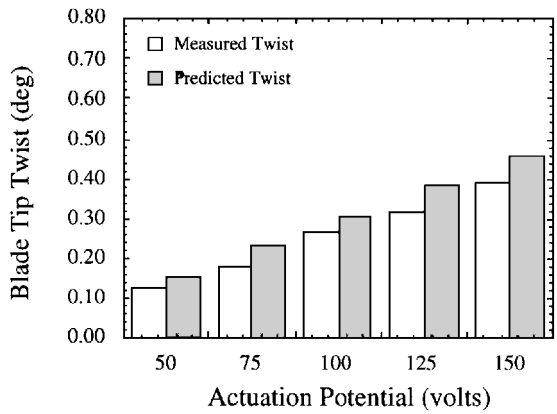

b) Blade 2A2 (ΔS = 1.5 in.)

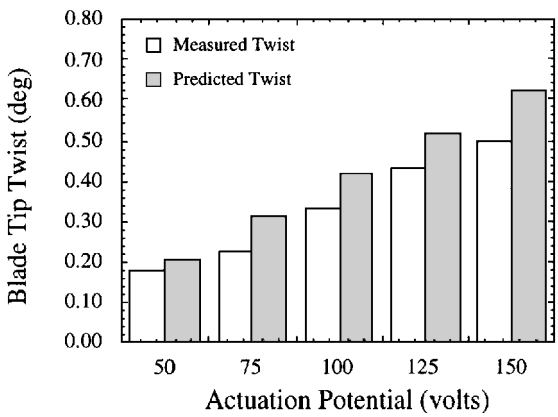

c) Blade 2B1 (ΔS = 0.75 in.)

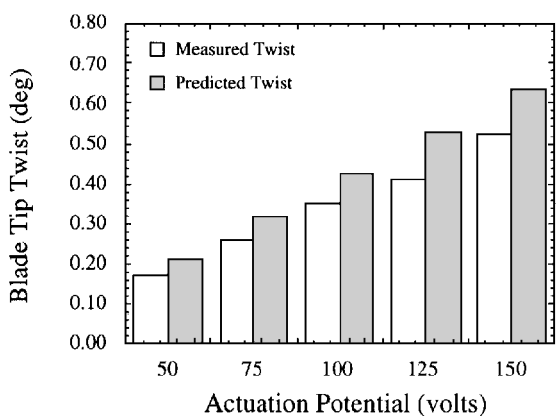

d) Blade 2B2 (ΔS = 0.75 in.)

Fig. 3 Static-induced torsional response of blades with dual-layered actuators.

attached to the blade tip. The flap, lag, and torsional modes of the blade were excited independently by an impulse hammer and the transient response was examined. The second torsional frequency was not resolvable due to flap/torsion coupling motion. The flap and fundamental torsion frequencies were also verified by examining the spanwise deflections of the blade under independent flap and torsion piezoactuation. These results are shown in Table 3. Each rotor configuration consists of two blades with similar parameters. Rotor 1A consists of blades 1A1 and 1A2; rotor 1B consists of blades 1B1 and 1B2; rotor 2A consists of blades 2A1 and 2A2; and rotor 2B consists of blades 2B1 and 2B2.

Nonrotating Blade Dynamic Response

Prior to hover testing, the nonrotating dynamic response of the blades was determined for each of the two blades of the four different rotor configurations. Excitation potentials of 100 V rms from 5 to 100 Hz were applied to the actuators to induce blade twist response. The frequency response of blade 2B1 is shown in Fig. 5. The trends were similar for all of the other blades. The amplitude of the peaks in twist response, as well as the amplitudes at nonresonant frequencies, are inversely proportional to the torsional stiffness GJ. In general, the off-resonant dynamic twist amplitudes of all of the blades were close to the predicted static values. This suggests that a static response analysis is adequate for predicting the off-resonant responses of the rotor blades.

Table 3 Rotor blade natural frequencies

	Frequency, Hz				
Rotor no.	First flap	Second flap	First torsion	First lag	Second lag
1A	4.4	25.0	70.0	9.8	89.0
1B	5.3	29.0	74.0	10.7	91.0
2A	4.0	24.1	72.0	8.9	89.2
2B	5.1	28.0	66.0	20.2	91.0

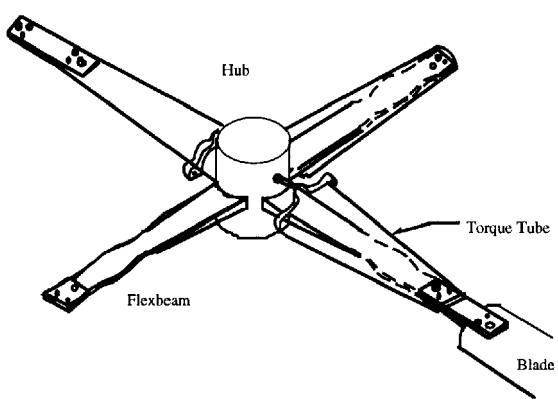

Fig. 4 Bearingless rotor model.

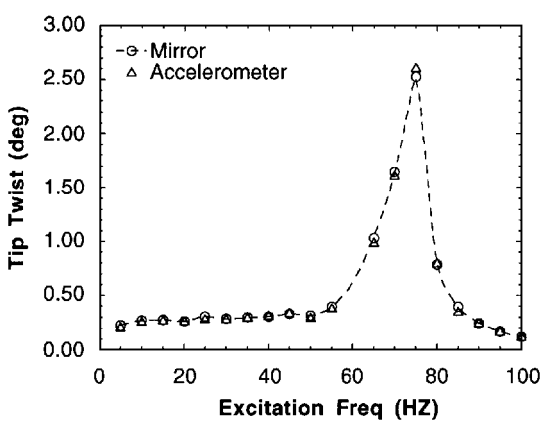

Fig. 5 Nonrotating dynamic induced twist response at 100 V rms excitation for blade 1B1 (30 single-layer actuators, $\Delta S = 0.75$ in.).

To resolve rotating tip twist amplitudes, two microaccelerometers (Entran EGAX-10) were embedded in the blade tips. The accelerometers were equally spaced from the elastic axis along the chord of the blade. The sensitivity axes were aligned perpendicular to the chord to sense the flap vertical response of the blade. To decouple flap/twist motions, a difference amplifier was used to electronically subtract the output signals from the two accelerometers. The net output signal was then processed by an FFT spectrum analyzer. This allowed for the determination of blade tip twist amplitudes at discrete excitation frequencies due to piezoactuation.

To ensure accurate twist measurements by the accelerometers, calibrations were completed for blade no. 1 of each rotor configuration using a laser/mirror optics system. An approximate error of less

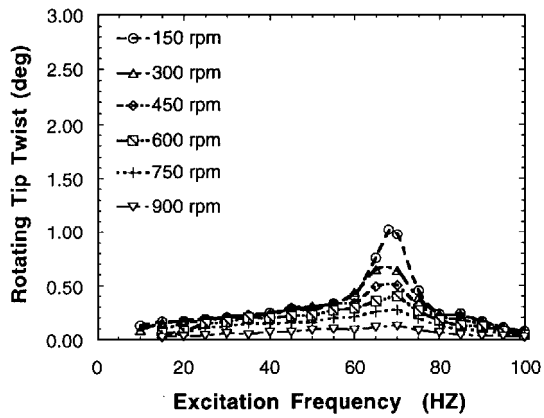

a) Blade 1A1 rotating twist response at 4-deg rotor collective

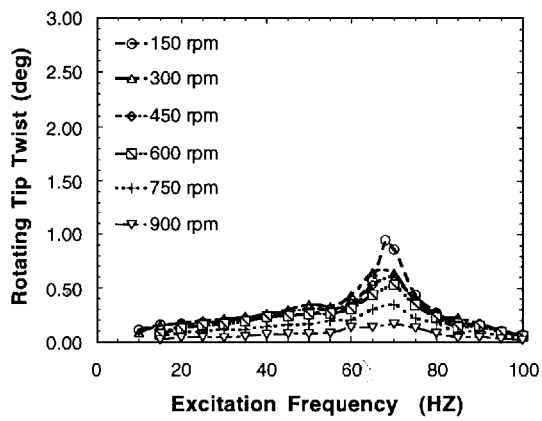

b) Blade 1A1 rotating twist response at 6-deg rotor collective

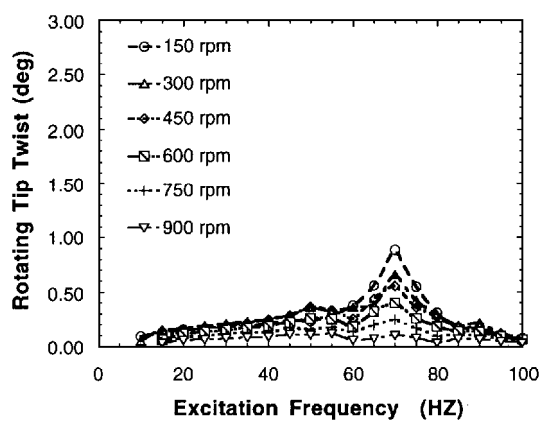

c) Blade 1A1 rotating twist response at 8-deg rotor collective

Fig. 6 Rotating dynamic induced twist response at 100 V rms excitation for blades with single-layer actuators ($\Delta S = 1.5$ in.) at various rotor collective angles.

than 3% in twist resolution was observed for off-resonant frequencies from 10 to 100 Hz (Fig. 5). The accelerometers were unable to accurately resolve twist amplitudes at the torsional resonance condition due to accelerations that exceeded the operational range ($\pm 10\,g$) of the EGAX-10 accelerometers.

Rotor Blade Rotating Response

Next, the four rotor configurations were tested on the hover stand at rotational speeds of 150, 300, 450, 600, and 750 and the Froude-scale operating speed of 900 rpm. The rotor collective pitch was set at 4, 6, and 8 deg and the piezoactuators were activated at 100 V rms at frequencies from 10 to 100 Hz to manipulate blade twist motion. The tip twist amplitudes of blade no. 1 of each rotor configuration were determined using the embedded accelerometers in conjunction with an FFT spectral analyzer.

The tip twist response data of blades 1A1 at 4, 6, and 8 deg collective pitch are shown in Fig. 6. The twist amplitudes at off-resonant frequencies are relatively constant and increase dramatically near resonance (approximately 70 Hz). Although blade 1A1 had significant nonrotating free displacements, the torsional response amplitudes were precipitously reduced by centrifugal and aerodynamic forces. In general, the response was observed to decrease in amplitude with increasing rpm for all collectives. The nominal twist amplitude for all collective settings at off-resonant activation frequencies is observed to be approximately 0.1 deg at 900 rpm. The twist response was also observed to reduce slightly

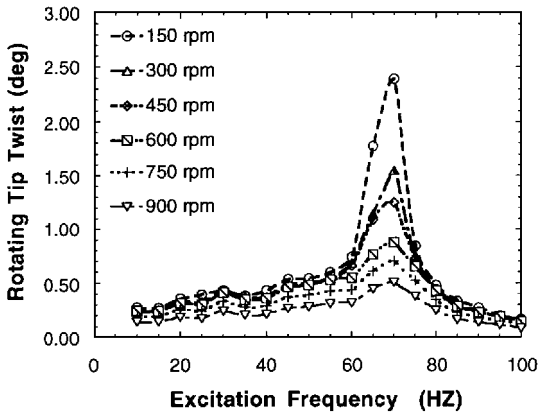

a) Blade 1B1 rotating twist response at 4-deg rotor collective

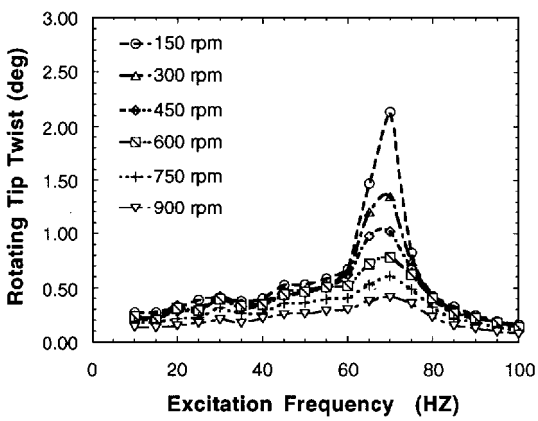

b) Blade 1B1 rotating twist response at 6-deg rotor collective

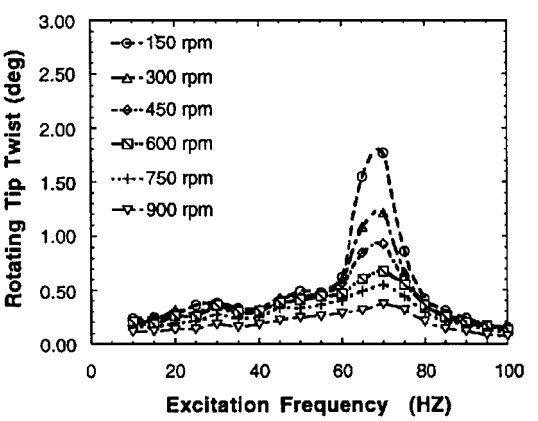

c) Blade 1B1 rotating twist response at 8-deg rotor collective

Fig. 7 Rotating dynamic induced twist response at 100 V rms excitation for blades with single-layer actuators (ΔS = 0.75 in.) at various rotor collective angles.

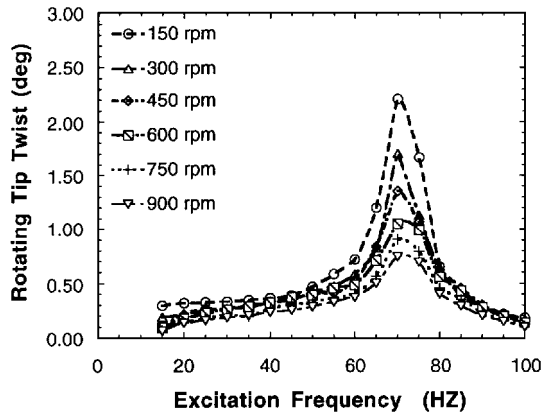

a) Blade 2A1 rotating twist response at 4-deg rotor collective

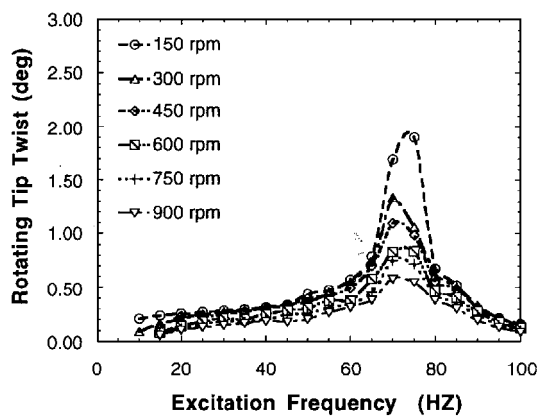

b) Blade 2A1 rotating twist response at 6-deg rotor collective

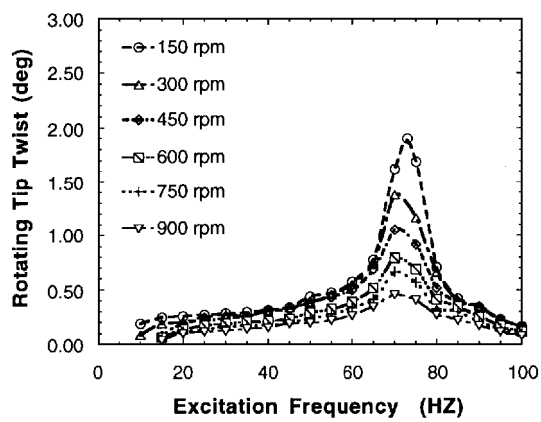

c) Blade 2A1 rotating twist response at 8-deg rotor collective

Fig. 8 Rotating dynamic induced twist response at 100 V rms excitation for blades with dual-layer actuators (ΔS = 1.5 in.) at various rotor collective angles.

with increasing collective. This effect is caused by the additional stresses on the piezoactuators due to blade bending at the higher lift conditions.[20]

The twist response data of blades 1B1 measured at 4, 6, and 8 deg rotor collective are shown in Fig. 7. Again, the twist response was observed to decrease with increasing rpm, as well as increasing collective pitch. However, an increase in the total number of actuators increases the block force, or ability of the actuators to deflect the blade in the presence of large external forces. Blade 1B1 achieved larger twist deflections (on the order of 0.2 deg) at 900 rpm as compared with blade 1A1. Similar trends were observed for the two-layer actuator configurations, blades 2A1 and 2B1 (Figs. 8 and 9, respectively). In general, the dual-layer actuator blade configurations achieved higher twist deflections than blade single-layer actuator blades. The maximum off-resonant twist response was measured for blade configuration 2B (on the order of 0.3 deg at 900 rpm).

An increase in the actuator thickness from one to two layers also results in higher block force. Blade 2A1 maintains significantly larger deflections at 900 rpm than blade 1A1. Similar increases were observed when comparing the twist deflections of blades 2B1 and 1B1. In general, the dual-layer actuators achieved higher blade twist deflections than the same number of single-layer actuators at 900 rpm.

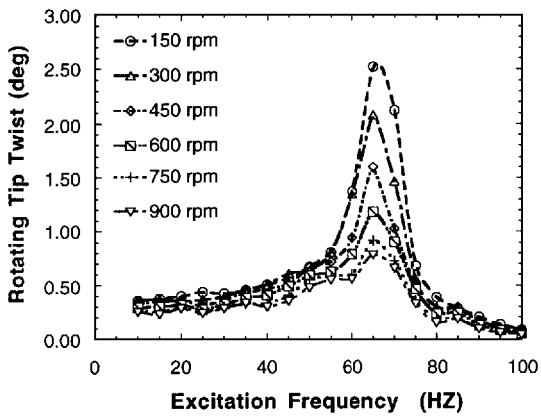

a) Blade 2B1 rotating twist response at 4-deg rotor collective

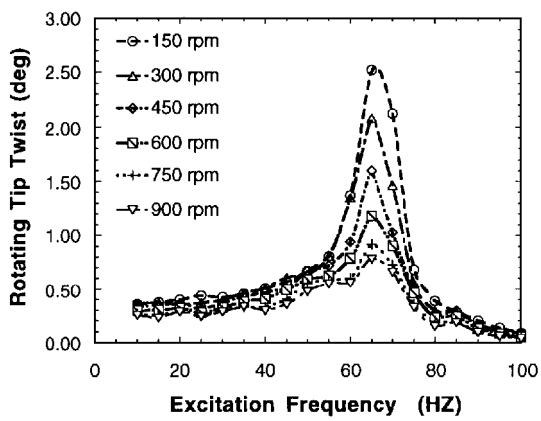

b) Blade 2B1 rotating twist response at 6-deg rotor collective

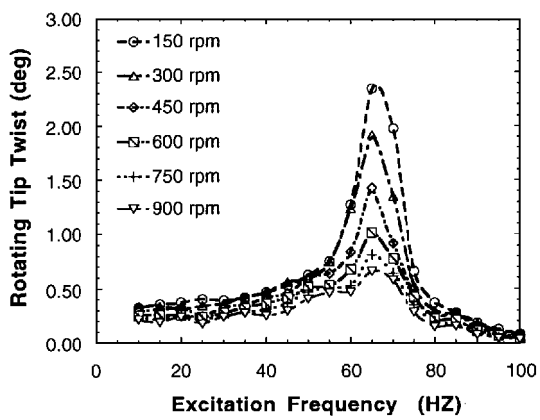

c) Blade 2B1 rotating twist response at 8-deg rotor collective

Fig. 9 Rotating dynamic induced twist response at 100 V rms excitation for blades with dual-layer actuators ($\Delta S = 0.75$ in.) at various rotor collective angles.

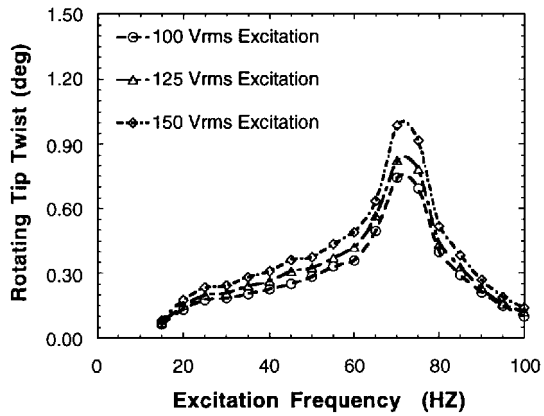

a) Blade 1B1 rotating twist response at 4-deg rotor collective

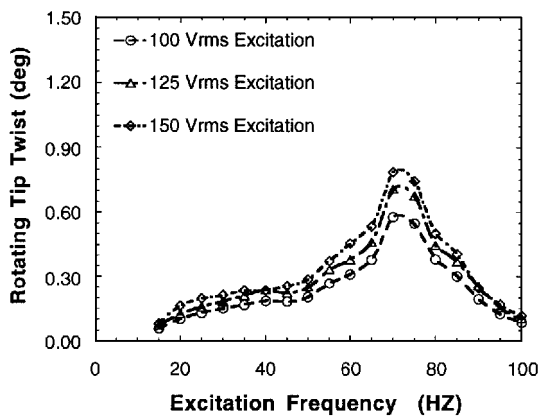

b) Blade 1B1 rotating twist response at 6-deg rotor collective

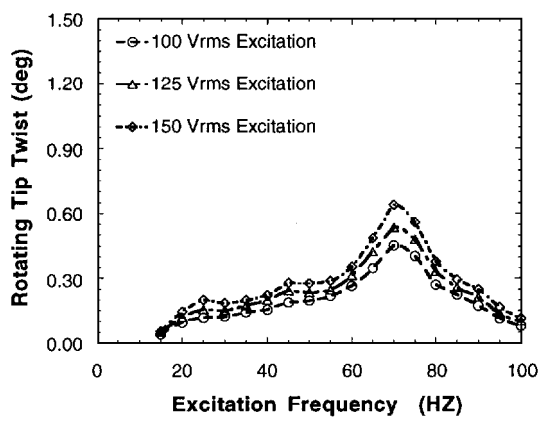

c) Blade 1B1 rotating twist response at 8-deg rotor collective

Fig. 10 Rotating dynamic induced twist response at 100 V rms excitation for blades with single-layer actuators ($\Delta S = 0.75$ in.) at various excitation voltages (900 rpm).

Hub Balance Results

To further assess the feasibility of a smart rotor, a rotating hub balance was used to measure the lift forces generated by oscillatory blade twist. The rotor was tested at three different collective settings of 4, 6, and 8 deg and for each case the blades were excited at higher harmonics of the rotational speed (1, 2, 3, and 4 /rev). The hub balance lift force and the tip twist were simultaneously measured to verify the trends and magnitudes of the lift force and blade twist. To generate significant lift forces at the test speed of 900 rpm, the actuators were excited at higher voltage potentials of 125 and 150 V rms. Using a specially conditioned sinusoidal input with a Trek 50/750 amplifier, a dc offset of 70 V was applied to maintain acceptably low tensile stresses in the PZT actuators (since piezoceramics typically fail in tension). An attempt was made to measure the increases in the oscillatory lift force at the twist excitation frequency for all four rotor configurations. However, because the nominal twist amplitudes for rotor 1A were relatively small, no significant change in lift force beyond background noise levels could be measured. The results for the three other rotor configurations are presented next.

Figures 10–12 show the twist response measured for the various rotor configurations at three collective pitch settings (4, 6, and 8 deg) and three activation voltages (100, 125, and 150 V rms). In general, the twist amplitudes for all collectives increase by approximately 20 and 15% as the excitation voltages are increased from 100 to 125 and 125 to 150 V rms, respectively. This behavior suggests that voltages in excess of 100 V rms will no longer result in a proportionate increase in twist. At these high voltages, the actuator strain, and hence the blade twist response, becomes

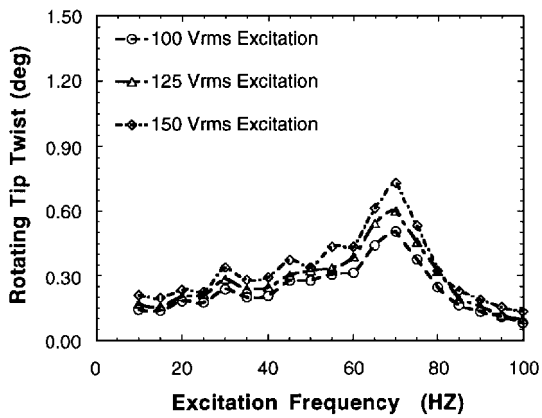

a) Blade 2A1 rotating twist response at 4-deg rotor collective

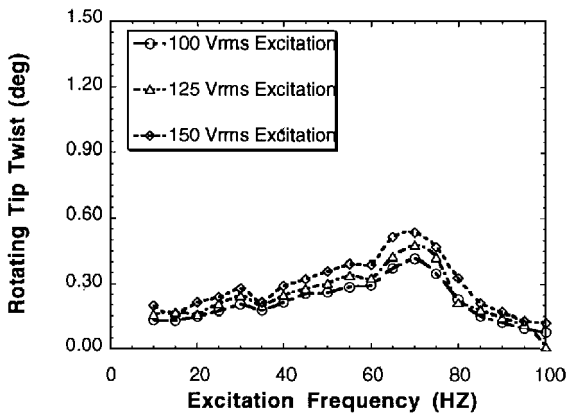

b) Blade 2A1 rotating twist response at 6-deg rotor collective

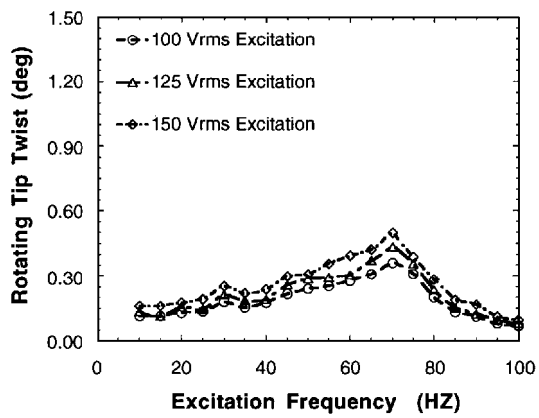

c) Blade 2A1 rotating twist response at 8-deg rotor collective

Fig. 11 Rotating dynamic induced twist response at 100 V rms excitation for blades with dual-layer actuators (ΔS = 1.5 in.) at various excitation voltages (900 rpm).

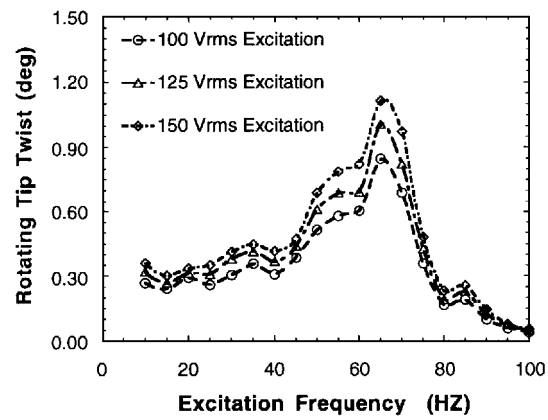

a) Blade 2B1 rotating twist response at 4-deg rotor collective

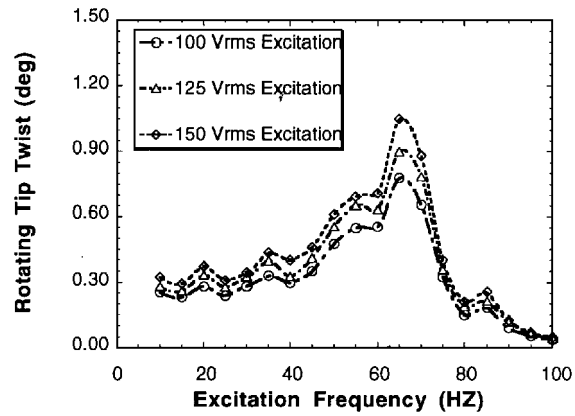

b) Blade 2B1 rotating twist response at 6-deg rotor collective

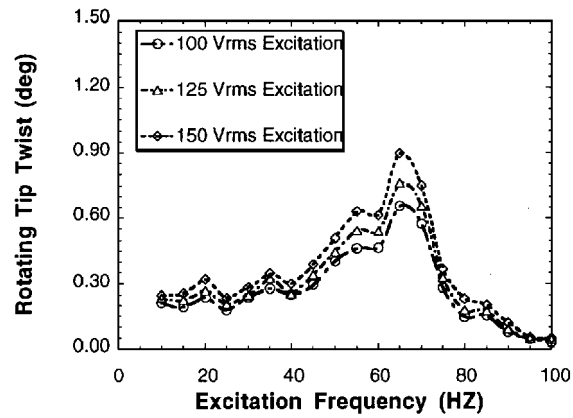

c) Blade 2B1 rotating twist response at 8-deg rotor collective

Fig. 12 Rotating dynamic induced twist response at 100 V rms excitation for blades with dual-layer actuators (ΔS = 0.75 in.) at various excitation voltages (900 rpm).

a nonlinear function of the applied field.[20] As seen in previous cases, the overall twist response decreases with increasing collective pitch.

The increases in oscillatory hub lift force due to harmonic blade twist excitation for rotor configuration 1B are shown in Fig. 13. The oscillatory lift force lift forces due to pitch excitation at the first four rotor harmonics are quite frequency dependent. The oscillatory lift forces are proportional to the twist amplitudes, being larger near the blade torsional resonance due to magnitude amplification. In addition, the oscillatory lift forces increase at higher blade twist activation voltages due to higher blade twist deflections. The nominal rotor lift at 4, 6, and 8 deg collective were measured to be approximately 7.3, 12.4, and 17.9 lb, respectively. During hover testing, the maximum changes in oscillatory lift amplitudes at 900 rpm were measured to be up to 10, 5, and 3% of the nominal steady-state lift force (150 V rms excitation) at 4, 6, and 8 deg rotor collectives, respectively. This decrease piezo-induced oscillatory lift force with increased rotor collective pitch is due to the additional bending stresses on the piezoceramic actuators at higher lift conditions.

The balance results for rotor 2A are shown in Fig. 14. Again, there is dynamic amplitude magnification near blade torsional resonance. In general, the magnitudes of lift for this configuration are smaller than those of rotor 1B. Oscillatory lift amplitudes of up to 8, 4, and 3% of the nominal rotor lift at 4, 6, and 8 deg collectives, respectively, were measured for this configuration at 900 rpm.

The hub balance results for rotor 2B are shown in Fig. 15. Because rotor lift is proportional to blade pitch, the change in oscillatory rotor lift due to piezoactuated blade pitch for this rotor configuration is the largest among all of the configurations tested. The maximum

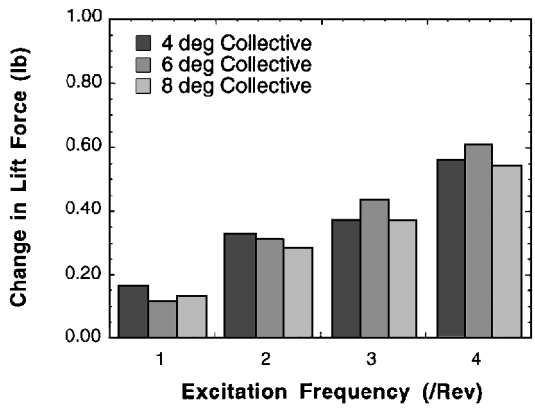

a) 100 V rms excitation

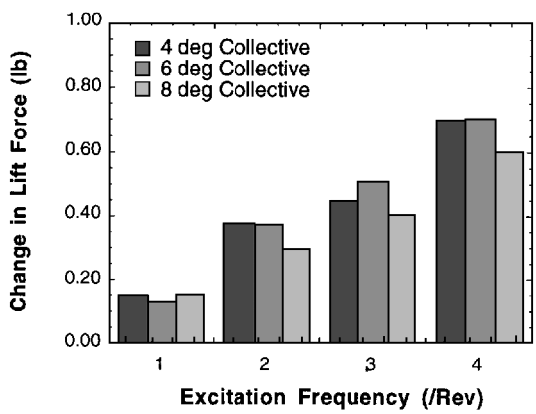

b) 125 V rms excitation

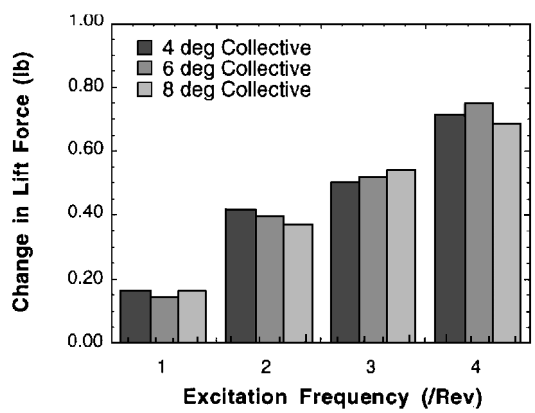

c) 150 V rms excitation

Fig. 13 Rotor 1B oscillatory hub lift force at various excitation voltages (900 rpm).

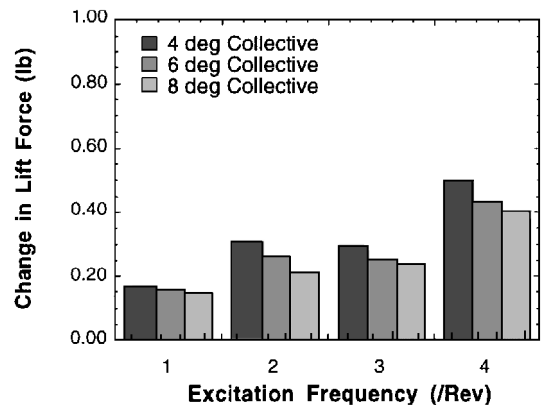

a) 100 V rms excitation

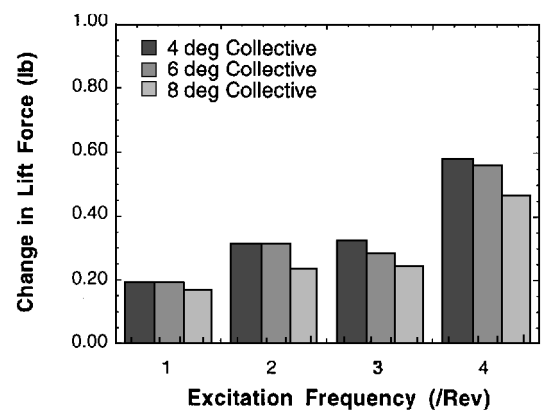

b) 125 V rms excitation

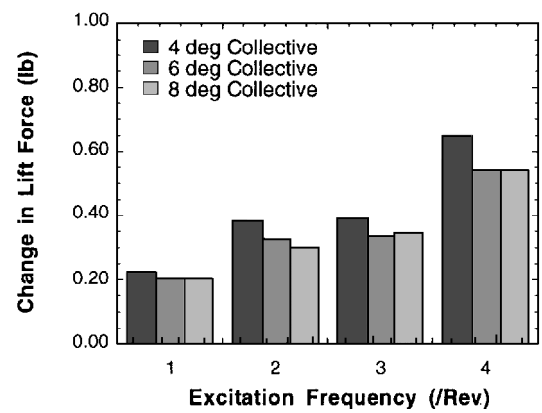

c) 150 V rms excitation

Fig. 14 Rotor 2A oscillatory hub lift force at various excitation voltages (900 rpm).

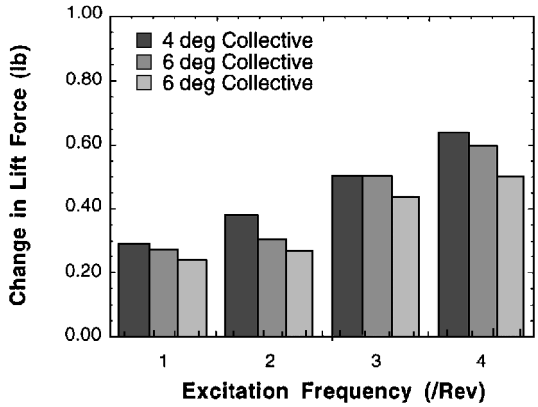

a) 100 V rms excitation

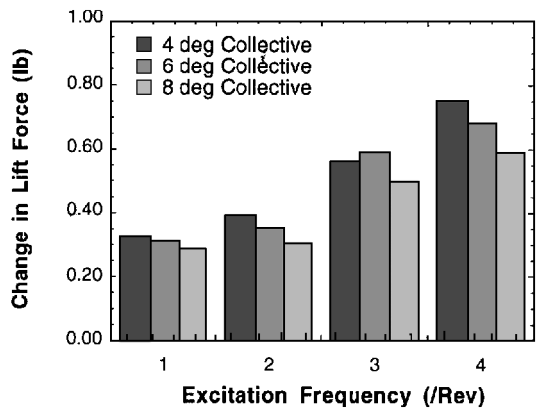

b) 125 V rms excitation

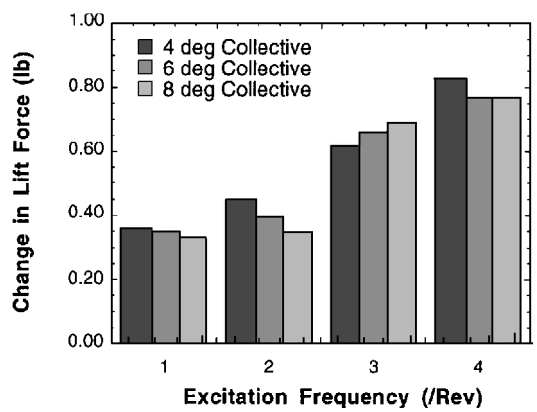

c) 150 V rms excitation

Fig. 15 Rotor 2B oscillatory hub lift force at various excitation voltages (900 rpm).

change in oscillatory lift at 150 V rms was measured to be up to 10, 6, and 4% of the nominal rotor lift at 4, 6, and 8 deg collectives, respectively.

Conclusions

This study examines the feasibility of a controllable twist Froude-scale rotor with embedded piezoceramic actuators. In this investigation, four actuator configurations were tested for static and hover twist response: 12 and 30 single-layer actuators and 12 and 30 dual-layer actuators. Several important observations were made: 1) actuator geometric parameters have a significant effect on the structural properties and hence the twist performance of the blades; 2) blade twist performance in static and hover modes differs due to the presence of large external loads at high rpm; 3) considerable changes in oscillatory hub loads occur due to piezoactuated blade. These observations are discussed in detail next.

The actuator parameters (i.e., number and thickness) have a significant effect on the structural properties of the blade. Specifically, increasing the number of actuators results in an increase in the torsional structural stiffness of up to 22%. This behavior is due to the ply stiffening effect with the PZT actuators, which account for the majority of the blade's torsional stiffness. The increase in blade torsional stiffness due to doubled actuator thickness, however, is not as large (up to 14% was measured).

Although blades with 12 single-layer actuators attained relatively larger free twist deflections, these amplitudes quickly diminished as the aerodynamic and centrifugal forces were increased due to higher rotational speeds. By increasing the number of single-layer actuators from 12 to 30, the twist deflections were increased at higher rotational speeds, although this was accomplished at the expense of a large increase in structural stiffness. To increase the actuator authority without significantly increasing the structural stiffness, single-layer actuators were replaced with dual-layer actuators to produce a higher actuation force. This results in higher block force to counteract large external loads. The maximum twist response at 900 rpm was attained by blades with 30 dual-layer actuators.

These results suggest that further efforts must be made to determine the optimal actuator configuration required to achieve maximum twist control authority at the Froude-scale rotor operating speed. At this time, the maximum twist deflection amplitudes on the order of 0.5 deg are attainable at 900 rpm for blades with dual-layer actuators.

Although the blade twist amplitudes were relatively small, significant unsteady airloads were generated at the Froude-scale operating speed. These test results demonstrate that piezoactuated blade twist is capable of altering the aerodynamics characteristics of the rotor. It is speculated that this blade actuation scheme could be used to generate new oscillatory airloads on the blade to cancel out blade vibrations at the source. For viable vibration control applications, 1–2 deg of blade tip twist is required at 900 rpm. However, at the present time, only partial vibration reduction may be feasible with the existing rotor configurations.

Acknowledgments

This work was supported in part by the U.S. Army Research Office under Grant DAAL 03-92-G-0121 with Gary Anderson as Technical Monitor. The authors would also like to thank Jon Velapoldi for his assistance in manufacturing and testing of rotor models.

References

[1] Loewy, R. G., "Helicopter Vibrations: A Technical Perspective," *Journal of the American Helicopter Society*, Vol. 29, No. 4, 1984, pp. 4–30.

[2] Chopra, I., and McCloud, J. C., III, "A Numerical Simulation Study of Open-Loop, Closed Loop and Adaptive Multicyclic Control Systems," *Journal of the American Helicopter Society*, Vol. 28, No. 1, 1983, pp. 311–325.

[3] Nguyen, K., and Chopra, I., "Application of Higher Harmonic Control (HHC) to Hingeless Rotor Systems," *Vertica*, Vol. 14, No. 14, 1990, pp. 545–556.

[4] Hammond, C. E., "Wind Tunnel Results Showing Rotor Vibratory Loads Reduction Using Higher Harmonic Blade Pitch," *Journal of the American Helicopter Society*, Vol. 28, No. 1, 1983, pp. 10–15.

[5] Miao, W., Kottapalli, S. B. R., and Frye, H. M., "Flight Demonstration of Higher Harmonic Control (HHC) on S-76," *Proceedings of the 42nd American Helicopter Society Forum* (Washington, DC), American Helicopter Society, Alexandria, VA, 1986.

[6] Straub, F. K., "A Feasibility Study of Using Smart Materials for Rotor Control," *Proceedings of the 49th Annual Forum of the American Helicopter Society* (St. Louis, MO), American Helicopter Society, Alexandria, VA, 1993.

[7] Chopra, I., "Development of a Smart Rotor," *Proceedings of the Nineteenth European Rotorcraft Forum* [Cernobbio (Como), Italy], 1993.

[8] Chen, P. C., and Chopra, I., "A Feasibility Study to Build a Smart Rotor: Induced-Strain Actuation of Airfoil Twist Using Piezoceramic Crystals," *Proceedings of the SPIE North American Conference on Smart Structures and Materials* (Albuquerque, NM), International Society for Optical Engineering, Bellingham, WA, 1993.

[9] Chen, P. C., and Chopra, I., "Torsion Modeling of a Smart Rotor with Induced-Strain Actuation of Blade Twist," *Proceedings of the American Helicopter Society National Technical Specialists' Meeting on Rotorcraft Structures* (Williamsburg, VA), American Helicopter Society, Alexandria, VA, 1995.

[10] Bothwell, M. C., Chandra, R., and Chopra, I., "Torsional Actuation with Extension-Torsion Composite Coupling and a Magnetostrictive Actuator," *AIAA Journal*, Vol. 33, No. 4, 1994, pp. 723–729.

[11] Walz, C., and Chopra, I., "Design and Testing of a Helicopter Rotor Model with Smart Trailing Edge Flaps," *Proceedings of the AIAA/ASME/ASCE/AHS 35th Structures, Structural Dynamics, and Materials Conference, Adaptive Structures Forum* (Hilton Head, SC), AIAA, Washington, DC, 1994.

[12] Ben-Zeev, O., and Chopra, I., "Development of an Improved Helicopter Rotor Model with Smart Trailing-Edge Flaps for Vibration Suppression," *Proceedings of the SPIE's North American Conference on Smart Structures and Integrated Systems* (San Diego, CA), International Society for Optical Engineering, Bellingham, WA, 1995.

[13] Crawley, E. F., and de Luis, J., "Use of Piezoceramic Actuators as Elements of Intelligent Structures," *AIAA Journal*, Vol. 25, No. 10, 1987, pp. 1373–1385.

[14] Crawley, E. F., and Anderson, E. H., "Detailed Modeling of Piezoceramic Actuation Beams," *Journal of Intelligent Material Systems and Structures*, Vol. 1, No. 1, 1990, pp. 4–25.

[15] Crawley, E. F., and Lazarus, K. B., "Induced Strain Actuation of Isotropic and Anisotropic Plates," *AIAA Journal*, Vol. 29, No. 6, 1991, pp. 944–951.

[16] Park, C., Walz, C., and Chopra, I., "Bending and Torsion Models of Beams with Induced Strain Actuators," *Proceedings of the SPIE North American Conference on Smart Structures and Materials* (Albuquerque, NM), International Society for Optical Engineering, Bellingham, WA, 1993.

[17] Park, C., and Chopra, I., "Modeling Piezoceramic Actuation of Beams in Torsion," *Proceedings of the AIAA/ASME/ASCE/AHS 35th Structures, Structural Dynamics, and Materials Conference, Adaptive Structures Forum* (Hilton Head, SC), AIAA, Washington, DC, 1994.

[18] Chen, P. C., and Chopra, I., "Induced Strain Actuation of Composite Beams and Rotor Blades with Embedded Piezoceramic Elements," *Journal of Smart Structures and Materials*, Vol. 3, No. 5, 1996, pp. 35–48.

[19] Anon., "Guide to Modern Piezoelectric Ceramics," Manufacturer's Product Data Sheet, Electro Ceramics Div., Morgan Matroc, Inc., Bedford, OH, March 1993.

[20] Chen, P. C., "Development of a Smart Rotor with Induced-Strain Actuation of Blade Twist," Ph.D. Dissertation, Dept. of Aerospace Engineering, Univ. of Maryland, College Park, MD, 1996.